

1 **Nipah virus matrix protein influences fusogenicity and is essential for particle**  
2 **infectivity and stability**

3 Erik Dietzel<sup>a</sup>, Larissa Kolesnikova<sup>a</sup>, Bevan Sawatsky<sup>b,c</sup>, Anja Heiner<sup>a</sup>, Michael Weis<sup>a</sup>, Gary P.  
4 Kobinger<sup>d,e,f</sup>, Stephan Becker<sup>a,g</sup>, Veronika von Messling<sup>b,c,g</sup>, and Andrea Maisner<sup>a#</sup>

5

6

7 <sup>a</sup> Institute of Virology, Philipps University Marburg, Marburg, Germany

8 <sup>b</sup> INRS-Institut Armand-Frappier, University of Quebec, Laval, Quebec, Canada

9 <sup>c</sup> Veterinary Medicine Division, Paul-Ehrlich-Institute, Langen, Germany

10 <sup>d</sup> National Microbiology Laboratory, Public Health Agency of Canada, Winnipeg, Manitoba,  
11 Canada

12 <sup>e</sup> Department of Medical Microbiology, University of Manitoba, Winnipeg, Manitoba, Canada

13 <sup>f</sup> Department of Immunology, University of Manitoba, Winnipeg, Manitoba, Canada

14 <sup>g</sup> German Center for Infection Research, Partner Site Giessen-Marburg-Langen, Germany

15

16

17 Running title: NiV M protein required for infectivity and stability

18

19 # Address correspondence to Andrea Maisner, maisner@staff.uni-marburg.de

20 Institute of Virology, Hans-Meerwein-Str. 2, 35043 Marburg, Germany

21

22

23 **ABSTRACT**

24 Nipah virus (NiV) causes fatal encephalitic infections in humans. To characterize the role of  
25 the matrix (M) protein in the viral life cycle, we generated a reverse genetics system based  
26 on the NiV Malaysia strain. Using an eGFP-expressing matrix (M) protein-deleted NiV, we  
27 observed a slightly increased cell-cell fusion, slower replication kinetics and significantly  
28 reduced peak titers compared to the parental virus. While increased amounts of viral  
29 proteins were found in the supernatant of cells infected with M-deleted NiV, the infectivity-  
30 to-particle ratio was more than 100-fold reduced, and the particles were less thermostable  
31 and of more irregular morphology. Taken together, our data demonstrate that the M protein  
32 is not absolutely required for the production of cell-free NiV, but is necessary for proper  
33 assembly and release of stable infectious NiV particles.

34

35 **IMPORTANCE**

36 Henipaviruses cause a severe disease with high mortality in human patients. Therefore,  
37 these viruses can only be studied in BSL-4 laboratories, making it more challenging to  
38 characterize their life cycle. Here we investigated the role of the Nipah virus matrix protein  
39 in virus-mediated cell-cell fusion and in the formation and release of newly produced  
40 particles. We found that even though low levels of infectious viruses are produced in the  
41 absence of the matrix protein, it is required for the release of highly infectious and stable  
42 particles. Fusogenicity of matrix-less viruses was slightly enhanced, further demonstrating  
43 the critical role of this protein in different steps of Nipah virus spread.

44

45 **INTRODUCTION**

46 Nipah virus (NiV) is a zoonotic paramyxovirus in the *Henipavirus* genus that originates from  
47 *Pteropus* bats. It causes sporadic outbreaks of deadly encephalitic disease in humans in  
48 Malaysia, Singapore, India and Bangladesh (1, 2). Cross-reactive antibodies against NiV and  
49 other related henipaviruses have been detected in bats and pigs as far afield as Africa and  
50 other parts of Southeast Asia, indicating that these viruses circulate quite widely (3-10).

51 NiV entry and cell-to-cell spread is driven by two transmembrane glycoproteins, the  
52 attachment (G) and the fusion (F) proteins, that are exposed on the surface of viral particles  
53 and on infected cells to mediate attachment to the host cell receptor and membrane fusion,  
54 respectively. The viral matrix (M) protein associates with the inner leaflet of the plasma  
55 membrane mediating the contact between the ribonucleoprotein (RNP) complex and the  
56 surface glycoproteins. Though the detailed role varies between different viruses,  
57 paramyxoviral M proteins are generally considered the main drivers of assembly (11).  
58 Supporting the idea of a critical role in virus particle formation and budding, NiV M protein  
59 forms virus-like particles when expressed on its own (12, 13), and it drives apical assembly  
60 and budding of NiV virions in polarized epithelial cells (14). Trafficking of the NiV M is a  
61 complex process involving transit through the nucleus (15-18), despite replication occurring  
62 exclusively in the cytoplasm. When NiV M protein nuclear localization or export signals are  
63 interrupted, or if ESCRT pathway-interacting late domains are disrupted, NiV M proteins lose  
64 their ability to accumulate at the plasma membrane and no longer generate virus-like  
65 particles (12, 17, 19). Aside of the M protein, the NiV glycoproteins appear to also possess  
66 intrinsic budding capabilities (13), but their roles in viral egress remain unresolved.

67 So far, only two paramyxoviruses, measles virus (MV) and human respiratory syncytial virus  
68 (HRSV), have been successfully rescued without transcomplementation by plasmid-encoded

69 M protein (20, 21). We show here that a recombinant eGFP-expressing M protein-deficient  
70 NiV (NiVeGΔM) could be recovered and propagated in the absence of any exogenous M  
71 expression. NiVeGΔM was detected in the culture supernatant, though virus titers were up  
72 to 1000-fold lower than for the parental wild-type virus, and cell-free viruses were less  
73 stable at 37°C. NiVeGΔM also displayed enhanced fusion kinetics, suggesting that the M  
74 protein plays a role in downregulation of the F/G-mediated cell-cell fusion. Taken together,  
75 our data show that the M protein plays an important role for the correct assembly of  
76 infectious cell-free NiV particles and influences the kinetics of cell-associated spread of NiV  
77 infection.

78

79

80

## 81 MATERIALS AND METHODS

82 **Cells and viruses.** Vero 76 cells (ATCC #CRL1587) and 293 cells (ATCC #CRL1573) were  
83 cultivated in Dulbecco's modified Eagle's medium (DMEM) with 10% fetal calf serum (FCS),  
84 100 U of penicillin/ml, 0.1 mg of streptomycin/ml, and 4 mM glutamine (all Life  
85 Technologies). All virus recovery and NiV infection experiments were performed in the BSL-4  
86 containment at the Institute of Virology, Philipps University of Marburg, Germany.

87 **Generation of NiV full-length cDNA plasmids.** Expression plasmids containing the  
88 nucleoprotein (N), phosphoprotein (P), and polymerase (L) protein were a kind gift of Dr.  
89 Markus Czub. To amplify fragments spanning the leader, trailer, and untranslated regions  
90 (UTR), RNA isolated from Vero cells infected with the NiV Malaysia strain (GenBank Acc. No.  
91 NC 002728) was reverse transcribed using Superscript III (Invitrogen, Burlington, ON) using  
92 random hexamer primers. For the internal UTRs, the primers were chosen to include a

93 unique or partially unique restriction site in each flanking gene. To introduce the enhanced  
94 green fluorescent protein (eGFP) in an additional transcription unit between G and L, the PM  
95 UTR was duplicated, and inserted between the G and eGFP open reading frames, yielding  
96 pBRT7-NiVeG. The M gene-deleted derivative pBRT7-NiVeGΔM was produced by deleting  
97 the M open reading frame except for the stop codon to assure the rule-of-six.

98 **Recovery of recombinant viruses.** To recover recombinant Nipah viruses,  
99 semiconfluent 293 cells in 6-well plates were infected with MVA-T7 at a multiplicity of  
100 infection (MOI) of 1. After 1h at 37°C, medium was changed to 500μl OptiMEM. Then, cells  
101 were transfected with 0.75μg pTM1-NiV N, 0.05μg pTM1-NiV P, 0.4μg pTM1-NiV L, and 5μg  
102 pBR/T7-NiVeG or pBR/T7-NiVeGΔM, respectively, using Lipofectamine 2000 (Life  
103 Technologies). After 3 – 4 hours at 37°C, medium was changed to DMEM 2% FCS with  
104 glutamine and antibiotics. If necessary, fresh 293 cells were added and medium was changed  
105 after 1 and 3 days, and the supernatant was transferred onto Vero cells after 6-9 days. Virus  
106 was harvested when 70 – 90% of the Vero cells showed cytopathic effects.

107 **Virus titration, particle stability, and growth kinetics.** Virus titers were quantified by  
108 limited dilution method and expressed as 50% tissue culture infections doses (TCID<sub>50</sub>). To  
109 evaluate the particle stability, these titers were compared with titers obtained after 1 and 5  
110 day incubation at 4°C or 37°C, respectively. For growth kinetics, confluent Vero cells seeded  
111 in 6-well plates were infected at a MOI of 0.001. After 1 h at 37°C, cells were washed 3 – 5  
112 times, and samples from the supernatant were collected (t<sub>0</sub>). Additional samples were  
113 collected and titrated after 24, 48, and 72 h. To compare cell-free and cell-associated virus  
114 titers, the cell culture supernatant was removed after 48 h, cleared for 10 min at 15,000g  
115 and used to determine cell-free virus titers. Infected cells were scraped into OptiMEM and  
116 frozen at -80°C. After rapid thawing at 37°C, cell lysates were cleared by low-speed

117 centrifugation, and cell-associated infectivity in the supernatants released by the freeze-  
118 thaw cycle was quantified. Viral titers ( $n \geq 3$ ) were compared using an unpaired t-test,  
119 performed in Microsoft Excel using the "T.TEST" function.

120 **Live cell imaging.** To characterize the dissemination of the different viruses, Vero  
121 cells seeded in 35-mm  $\mu$ -dishes (Ibidi, Munich) were infected with NiVeG or NiVeG $\Delta$ M at a  
122 MOI of 0.005. After 1 h at 37°C, medium was replaced by CO<sub>2</sub>-independent Leibovitz's  
123 medium without phenol red (Life Technologies) with 100U/ml penicillin and 100 $\mu$ g/ml  
124 streptomycin, 20% FBS, and 400 $\mu$ M 6-hydroxy-2,5,7,8-tetramethylchromane-2-carboxylic  
125 acid (Trolox; Sigma). Live cell time-lapse experiments were started at 16 h after infection and  
126 recorded with a Leica DMI6000B microscope using a 20x objective equipped with a remote  
127 control device to operate the microscope from outside the BSL-4 facility. Pictures were taken  
128 every 30 min and processed with Leica LAS AF software. The increase in size of a syncytium  
129 as a parameter for fusion kinetics was determined by measuring the area of 12 individual  
130 syncytia at different time points using ImageJ (<http://rsbweb.nih.gov/ij>). To calculate the  
131 relative increase, the area of the syncytium at 17 h after infection was set as 1.

132 **MTT assay.** The MTT assay was performed according to the manufacturer's protocol  
133 (Thermo Fisher Vybrant MTT Cell Proliferation Assay Kit). Briefly, Vero cells grown in a 96-  
134 well plate were infected with NiVeG or NiVeG $\Delta$ M at a MOI of 0.001 or 0.01. After 2 days,  
135 medium was replaced by PBS containing 1 mM MTT. After incubation for 4 h at 37°C,  
136 supernatants were removed, mixed with DMSO and further incubated for 10 min at 37°C  
137 before absorption was measured at 562 nm using a PHOmo Microplate reader. To calculate  
138 the relative cytotoxicity, the absorbance of uninfected cells was set to 1.

139           **Quantification of NiV-N RNA.** Viral RNA was extracted from supernatants of NiVeG or  
140 NiVeGΔM-infected Vero cells using the RNeasy kit (Qiagen) and reverse transcribed using  
141 Revert Aid H Minus Reverse Transcriptase (Fermentas). Real time PCR reactions were  
142 performed in triplicates with a StepONE Plus cycler using QuantiFast SYBR green PCR Master  
143 Mix (Applied Biosystems) and NiV N specific diagnostic primers. Genome numbers ( $2^{-Ct}$ ), and  
144 the infectivity-to-particle ratio calculated by dividing the titer (TCID<sub>50</sub>/ml) by  $2^{-Ct}$ , was  
145 normalized to the values obtained for NiVeG (set as 1).

146           **Virus purification and Western blot analysis.** To evaluate viral protein expression  
147 levels, Vero cells were infected with NiVeG or NiVeGΔM at a MOI of 0.001. After 48 h, the  
148 supernatant was harvested and precleared by centrifugation for 10 min at 15,000g. Virus  
149 particles were then isolated by ultracentrifugation through a 20% Sucrose cushion for 1.5 h  
150 at 150,000g and subsequent resuspension of the pellet in 30 μl 1% sodium dodecylsulfate  
151 (SDS, Sigma) in phosphate-buffered saline (PBS, Life Technologies). Cell lysates were  
152 collected at the same time by scraping the cells into 1% SDS in PBS. Two % of the cell lysate  
153 and 33% of the virus pellet were then separated by reducing SDS-PAGE and transferred onto  
154 nitrocellulose. Membranes were incubated with polyclonal rabbit antisera directed against  
155 NiV G, F, and M peptides (G1126, F631, M1321; immunGlobe, Himmelstadt, Germany),  
156 followed by a biotin-labeled anti-rabbit antiserum and horseradish peroxidase-conjugated  
157 streptavidin (Amersham). Bands were detected using a ChemiDoc (BioRad). To stain NiV N,  
158 membranes were incubated with a polyclonal anti-NiV guinea pig serum (22). Primary  
159 antibodies were detected with an IRDye700-conjugated anti-guinea pig secondary antibody  
160 (LI-COR) and visualized with an Odyssey Imager (LI-COR).

161           **Proteinase K protection assay.**  $2 \times 10^6$  Vero cells were infected with NiVeG or  
162 NiVeGΔM at a MOI of 0.001. After 48 h, supernatants were cleared for 10 min at 15,000g

163 and subsequently centrifuged for 1 h at 150,000g. Virus pellets were resuspended in 60 $\mu$ l  
164 PBS. Twenty  $\mu$ l of the virus suspension was either left untreated (control), or was treated for  
165 30 min at 37°C with Proteinase K at a final concentration of 0.1 $\mu$ g/ $\mu$ l in the absence or  
166 presence of 1% Triton X-100. Digestion was stopped by the addition of 1  $\mu$ g/ $\mu$ l PMSF.  
167 Samples were then inactivated and subjected to Western blot analysis using the polyclonal  
168 anti-NiV guinea pig serum.

169 **Electron microscopy.** For each virus, Vero cells grown to confluency in three 175 cm<sup>2</sup>  
170 flasks were infected with NiVeG or NiVe $\Delta$ M at a MOI of 0.005. After 48 h, virus particles  
171 were purified as outlined above, and the pellets were resuspended in 150 $\mu$ l PBS. A drop of  
172 purified virus suspension was added on Formvar-coated nickel grids and incubated for 5 min.  
173 Then, samples were inactivated with 4% PFA for two days, and negative staining was  
174 performed with 2% phosphotungstic acid. Alternatively, grids were immuno-stained using a  
175 NiV-specific guinea pig serum and donkey anti-guinea pig secondary antibodies conjugated  
176 with 12 nm colloidal gold (Jackson ImmunoResearch; USA). Samples were analyzed by using  
177 a JEM 1400 transmission electron microscope at 120 kV.

178 **RESULTS**

179 **M gene-deleted NiV are released in the supernatant.** While non-infectious systems  
180 have contributed importantly to the characterization of the henipavirus life cycle, several  
181 fundamental questions can only be answered using recombinant viruses. So far, such  
182 genetically modified recombinant NiV have been either used to analyze the functions of V,  
183 W or C proteins (23-25), or to characterize chimeric viruses in which NiV genes were  
184 exchanged by the homologous Hendra virus (HeV) genes (26). Here, we generated a  
185 replicative M gene-deleted NiV to characterize assembly and budding of infectious cell-free  
186 NiV particles in the total absence of M. Towards this, we generated a reverse genetics  
187 system based on the strategy used for the related morbilliviruses (27, 28). The entire  
188 genome of the NiV Malaysia strain was assembled in a low copy plasmid and flanked by a T7  
189 promoter and a T7 terminator/hepatitis  $\delta$  ribozyme cassette to ensure correct genome ends  
190 (NiV, Fig. 1A). An additional transcription unit carrying the eGFP gene was introduced  
191 between the G and L genes (NiVeG) to facilitate the detection of infected cells. To generate  
192 an M-deleted virus (NiVeG $\Delta$ M), the M open reading frame was deleted from the NiVeG  
193 genomic plasmid (Fig. 1A).

194 All recombinant viruses could be recovered by transfecting the respective genomic plasmid  
195 with T7 polymerase-driven expression plasmids for the N, P, and L proteins in 293 cells  
196 previously infected with MVA-T7, which provided the T7 polymerase. Interestingly,  
197 NiVeG $\Delta$ M could be rescued and propagated without transcomplementation of plasmid-  
198 encoded M protein. While replication efficacies of recombinant NiV and NiVeG were similar,  
199 indicating that introduction of the GFP cassette did not affect virus growth (Fig. 1B),  
200 NiVeG $\Delta$ M was associated with ten- to thousand-fold lower titers (Fig. 1C). Since the maximal  
201 cell-associated infectivity was similarly reduced (Fig. 1D), this cannot be explained by just a

202 budding defect in the absence of M. Instead, it indicates that the M protein is required for  
203 proper assembly of infectious particles.

204 **Absence of M protein results in enhanced syncytia formation kinetics.** While  
205 deletion of Sendai or measles virus (MV) M genes caused an increased fusogenicity and  
206 resulted in the formation of much larger syncytia (20, 29), no influence on the cytopathic  
207 effect was observed for a human respiratory syncytial virus (HRSV) lacking the M protein  
208 (21). Phase contrast microscopy suggested a slightly enhanced fusogenicity of NiVeGΔM.  
209 However, because of the heterogeneous sizes of syncytia at any steady state time point after  
210 infection, the differences in average syncytia sizes were not statistically significant (data not  
211 shown). We therefore performed a live-cell imaging analysis of Vero cells infected with  
212 NiVeG and NiVeGΔM. By monitoring individual syncytia over two days, we analyzed fusion  
213 kinetics to determine the influence of M deletion on the progression of NiV-mediated cell-  
214 cell fusion. For both viruses, first syncytia encompassing 2-5 cells were detected 17 h after  
215 infection (Fig. 2A). There was a gradual increase in syncytia sizes over time for both viruses,  
216 but fusion kinetics was more pronounced for NiVeGΔM (Fig. 2B). Though syncytia generally  
217 grew faster due to the increased fusogenicity of NiVeGΔM, this did not result in an enhanced  
218 cytotoxic effect. Cell viability of NiVeG and NiVeGΔM-infected cells at 24 h and 48 h p.i. did  
219 not differ significantly (Fig. 2C). As in Vero cells, we observed an enhanced fusogenicity of  
220 NiVeGΔM in A549 cells (data not shown). Together, these results illustrate that the NiV M  
221 protein modulates glycoprotein-mediated cell-to-cell fusion to a greater extent than the M  
222 protein of HRSV, albeit to a lesser extent than the M proteins of Sendai virus or MV.

223 **M protein deletion causes formation of less infectious particles with reduced**  
224 **stability.** To determine if reduced NiVeGΔM titers are the result of less efficient particle  
225 formation, or of a difference in particle infectivity, we compared the amount of viral RNA in

226 the supernatant of NiVeG or NiVeGΔM-infected cells, in which infectious titers of the latter  
227 were about 100-fold reduced. Real-Time RT-PCR analysis (qPCR) with NiV-N specific primers  
228 revealed an increased relative particle/genome number in the supernatant of NiVeGΔM-  
229 infected cells (Fig. 3A, left panel). Setting the infectivity-to-particle ratio of NiVeG to 1,  
230 NiVeGΔM thus yielded a relative infectivity between 0.001 and 0.01 (Fig. 3A, right panel). To  
231 evaluate if differences in viral protein expression account for this observation, we analyzed  
232 the NiV protein expression in infected cell lysates and the particle composition. As expected,  
233 the M protein was absent in NiVeGΔM-infected cells and the resulting viral particles (Fig. 3B,  
234 lines 3 and 4). While the viral protein content in infected cells was otherwise not affected by  
235 the absence of M (Fig. 3B, lanes 1 and 3), the total amount of G, F, and N proteins in the  
236 purified viral particle fraction was considerably higher for NiVeGΔM (Fig. 3B, lanes 4 and 2).  
237 As shown in the Coomassie-stained gel (Fig. 3C), NiVeGΔM virus preparations not only  
238 contained higher amounts of viral proteins but also a substantially increased amount of total  
239 (cellular) proteins (Fig. 3C). Proteinase K (PK) digestion in the absence and presence of TX-  
240 100 confirmed that particles with incorporated N protein are present in NiVeG and NiVeGΔM  
241 supernatants (Fig. 3D). However, compared to PK-treated NiVeG particles, the relative  
242 amount of N protein in PK-digested NiVeGΔM particles was reduced. This might hint on a  
243 compromised viral membrane integrity when M is absent.

244 To assess if M depletion not only affects the composition of cell-free virus preparations but  
245 also their thermostability, we compared the infectivity of NiVeG and NiVeGΔM after  
246 incubation at 4°C or 37°C. While infectious titers of both viruses remained almost stable for  
247 5 days at 4°C, incubation for 24 h at 37°C had little effect on the parental NiVeG, but resulted  
248 in a statistically highly significant tenfold drop in titers for NiVeGΔM (Fig. 3E). After 5 days at  
249 37°C, infectivity of NiVeGΔM was reduced by more than hundredfold, while NiVeG titers had

250 only dropped tenfold (Fig. 3E). Taken together, this supports the idea that in the absence of  
251 M, the coordinated assembly of largely cell protein-free virus virions is disturbed, resulting in  
252 the production of cell-free NiVeGΔM particles with increased cellular protein incorporation  
253 and lower particle stability.

254 **The M protein coordinates the budding process.** To gain more detailed insights in  
255 the morphology of the released particles, we performed a negative-stain transmission EM  
256 analysis of cell-free virus preparations from NiVeG and NiVeGΔM-infected cell supernatants  
257 at 48 h after infection. Consistent with the detection of increased viral and cellular protein  
258 amounts by Western blot analysis and Coomassie staining (Fig. 3B and D), virus preparations  
259 pelleted from supernatants of NiVeGΔM-infected cells contained a dramatically increased  
260 amount of vesicular material compared to NiVeG virus preparations (Fig. 4A and B). For a  
261 more in depth characterization of the particle morphology, we analyzed NiVeG and  
262 NiVeGΔM samples by immuno-EM using a polyclonal anti-NiV guinea pig antiserum. In both  
263 virus preparations, we found particles heavily decorated with immunogold beads. Among  
264 them were spherical, filamentous and pleomorphic virions, as previously described by Hyatt  
265 et al. (30). Spherical NiVeG and NiVeGΔM particle sizes both ranged from 90 to 380 nm (Fig.  
266 4C and D), and filamentous NiVeG and NiVeGΔM particles also had similar total sizes (Fig. 4E  
267 and F). However, these elongated NiVeGΔM particles had a more irregular shape and  
268 displayed some defects in the particle envelope (Fig. 4F, arrows), what supports the idea of a  
269 compromised membrane integrity suggested by the PK digestion (Fig. 3D). Similar to  
270 filamentous particles, NiVeGΔM particles with pleomorphic shapes differed from  
271 pleomorphic NiVeG by a more irregular morphology, an uneven surface and some envelope  
272 blebs (Fig. 4G and H), indicating a less coordinated budding process in the absence of M.

273

274 **DISCUSSION**

275           The characterization of NiV assembly in the total absence of the M protein has thus  
276 far relied on the co-expression of recombinant proteins outside the authentic viral context.  
277 To address this limitation, we established a reverse genetics system based on the NiV  
278 Malaysia strain. Using the system, we were able to recover NiVeGΔM, an eGFP-expressing  
279 derivative lacking the M protein transcription unit. While the fusogenicity of NiVeGΔM was  
280 slightly enhanced, replication kinetics was significantly impaired. Together with the release  
281 of high amounts of viral and cellular proteins and the severely reduced infectivity and  
282 stability, our data indicate that the M protein is essential for proper NiV particle assembly,  
283 consistent with its role in other paramyxoviruses (21, 31-33).

284           **Requirements for virus-like particle and infectious particle formation are different.**

285           Virus-like particles (VLPs) are frequently used to investigate assembly mechanisms of  
286 enveloped viruses (34). For NiV, expression of the F or G proteins alone is sufficient to yield  
287 VLPs in the supernatant, and the co-expression of M greatly increases the efficiency of VLP  
288 formation (13, 35). This intrinsic budding activity of the F and G proteins is likely the origin of  
289 the large amount of viral protein detected in purified supernatant of NiVeGΔM-infected  
290 cells. However, the low infectivity-to-particle ratio indicates that these M protein-  
291 independent budding activities only accidentally generate infectious RNP-containing  
292 particles while mostly yielding non-infectious virus-like particles also found in F/G expression  
293 systems. Furthermore, it is likely that the envelope of the few RNP-containing particles  
294 produced in the absence of the M protein has a suboptimal composition of surface  
295 glycoproteins, which may impair the virus entry and uncoating processes (11, 21). Whether  
296 the role of the M protein in the assembly process is mainly to concentrate viral components

297 at specific sites at the plasma membrane or to ensure a defined stoichiometry of RNPs, G  
298 and F proteins requires further investigation.

299 **Conserved and divergent functions of paramyxovirus M proteins.**

300 Despite their conserved role in assembly and budding, there are genus- and strain-specific  
301 differences between paramyxoviral matrix proteins that do not allow exchanging M proteins  
302 even between closely related viruses without affecting virus growth (36-38). In line with  
303 these studies, a recent cross-complementation study of Yun et al. (26) demonstrated that  
304 introduction of the Hendra virus M gene into NiV increased the replicative titers, likely as a  
305 result of an increased budding activity of HeV M.

306 While some attempts to generate members of the *Paramyxoviridae* family without  
307 complementation of functional M proteins were not successful (31-33), M protein-deleted  
308 measles (MVΔM), and respiratory syncytial (M-null HRSV) viruses have been recovered (20,  
309 21). While M-null HRSV was completely defective in virus budding (21), limited amounts of  
310 infectious MVΔM were found in the supernatant (20), indicating a varying importance of the  
311 M protein contribution among different genera.

312 In line with what has been reported for MVΔM (20), we observed an increased fusogenicity  
313 for NiVeGΔM. Although the effect of M depletion on NiV-mediated cell-cell fusion is clearly  
314 less pronounced, it may be speculated that as in MV infection (39, 40), NiV M downregulates  
315 cell-cell fusion by interacting with the cytoplasmic portions of the NiV surface glycoproteins.

316 In contrast to the increased fusogenicity seen in M-deficient MV, Sendai virus and NiV,  
317 deletion of the HRSV M protein did not result in enhanced fusion (21), suggesting that  
318 paramyxovirus M proteins differentially influence cell-to-cell fusion. In polarized cell types,  
319 the role of M proteins might be even more diverse. Due to the polarized nature of epithelial  
320 and endothelial target tissues, viral proteins and RNPs are often specifically transported to

321 apical or basolateral membrane domains. In the case of NiV, NiV F and G proteins contain  
322 cytoplasmic sorting signals that lead to a basolateral targeting upon single expression. In the  
323 viral context, however, both glycoproteins are expressed in a more apical fashion. This  
324 redistribution is assumed to be caused by the NiV M that is selectively targeted to the apical  
325 surface of polarized cells (14, 41, 42). This M-driven apical accumulation of all viral  
326 components is thought to ensure efficient apical NiV budding while downregulating F/G-  
327 dependent lateral cell-to-cell fusion kinetics within the polarized cell monolayer. Future  
328 studies will determine the effect of M deficiency on unipolar NiV budding and fusion  
329 downregulation in polarized endothelial and epithelial cell types.

330

331

#### 332 **FUNDING INFORMATION**

333 This work was supported by CIHR grant MOP66989 and funding from the German Ministry of  
334 Health to V.v.M., and was funded by grants of the German Research Foundation (DFG) to A.  
335 M. (MA 1886/4-2 and SFB 1021 TP B04).

336 The funders had no role in study design, data collection and interpretation, or the decision  
337 to submit the work for publication.

338

#### 339 **ACKNOWLEDGEMENTS**

340 All work with live NiV was performed in the BSL-4 facility of the Philipps University, Marburg,  
341 Germany. We thank Markus Czub and Heinz Feldmann for providing NiV plasmids and guinea  
342 pig antisera. We also thank all laboratory members, especially Marc Ringel and Boris Lamp,  
343 for continuing support and lively discussions.

344

## 345 REFERENCES

- 346 1. **Chua KB, Goh KJ, Wong KT, Kamarulzaman A, Tan PS, Ksiazek TG, Zaki SR, Paul G, Lam SK,**  
347 **Tan CT.** 1999. Fatal encephalitis due to Nipah virus among pig-farmers in Malaysia. *Lancet*  
348 **354:1257-1259.**
- 349 2. **Luby SP, Hossain MJ, Gurley ES, Ahmed BN, Banu S, Khan SU, Homaira N, Rota PA, Rollin**  
350 **PE, Comer JA, Kenah E, Ksiazek TG, Rahman M.** 2009. Recurrent zoonotic transmission of  
351 Nipah virus into humans, Bangladesh, 2001-2007. *Emerg Infect Dis* **15:1229-1235.**
- 352 3. **Baker KS, Todd S, Marsh GA, Crameri G, Barr J, Kamins AO, Peel AJ, Yu M, Hayman DT,**  
353 **Nadjm B, Mtove G, Amos B, Reyburn H, Nyarko E, Suu-Ire R, Murcia PR, Cunningham AA,**  
354 **Wood JL, Wang LF.** 2013. Novel, potentially zoonotic paramyxoviruses from the African  
355 straw-colored fruit bat *Eidolon helvum*. *J Virol* **87:1348-1358.**
- 356 4. **Drexler JF, Corman VM, Gloza-Rausch F, Seebens A, Annan A, Ipsen A, Kruppa T, Müller**  
357 **MA, Kalko EK, Adu-Sarkodie Y, Oppong S, Drosten C.** 2009. Henipavirus RNA in African bats.  
358 *PLoS One* **4:e6367.**
- 359 5. **Hasebe F, Thuy NT, Inoue S, Yu F, Kaku Y, Watanabe S, Akashi H, Dat DT, Mai IT, Morita K.**  
360 2012. Serologic evidence of nipah virus infection in bats, Vietnam. *Emerg Infect Dis* **18:536-**  
361 **537.**
- 362 6. **Hayman DT, Suu-Ire R, Breed AC, McEachern JA, Wang L, Wood JL, Cunningham AA.** 2008.  
363 Evidence of henipavirus infection in West African fruit bats. *PLoS One* **3:e2739.**
- 364 7. **Hayman DT, Wang LF, Barr J, Baker KS, Suu-Ire R, Broder CC, Cunningham AA, Wood JL.**  
365 2011. Antibodies to henipavirus or henipa-like viruses in domestic pigs in Ghana, West Africa.  
366 *PLoS One* **6:e25256.**
- 367 8. **Lehle C, Razafitrimo G, Razainirina J, Andriaholinirina N, Goodman SM, Faure C, Georges-**  
368 **Courbot MC, Rousset D, Reynes JM.** 2007. Henipavirus and Tioman virus antibodies in  
369 pteropodid bats, Madagascar. *Emerg Infect Dis* **13:159-161.**
- 370 9. **Peel AJ, Baker KS, Crameri G, Barr JA, Hayman DT, Wright E, Broder CC, Fernández-Loras A,**  
371 **Fooks AR, Wang LF, Cunningham AA, Wood JL.** 2012. Henipavirus neutralising antibodies in  
372 an isolated island population of African fruit bats. *PLoS One* **7:e30346.**
- 373 10. **Reynes JM, Counor D, Ong S, Faure C, Seng V, Molia S, Walston J, Georges-Courbot MC,**  
374 **Deubel V, Sarthou JL.** 2005. Nipah virus in Lyle's flying foxes, Cambodia. *Emerg Infect Dis*  
375 **11:1042-1047.**
- 376 11. **El Najjar F, Schmitt AP, Dutch RE.** 2014. Paramyxovirus glycoprotein incorporation, assembly  
377 and budding: a three way dance for infectious particle production. *Viruses* **6:3019-3054.**
- 378 12. **Ciancanelli MJ, Basler CF.** 2006. Mutation of YMYL in the Nipah virus matrix protein  
379 abrogates budding and alters subcellular localization. *J Virol* **80:12070-12078.**
- 380 13. **Patch JR, Crameri G, Wang LF, Eaton BT, Broder CC.** 2007. Quantitative analysis of Nipah  
381 virus proteins released as virus-like particles reveals central role for the matrix protein. *Virol J*  
382 **4:1.**
- 383 14. **Lamp B, Dietzel E, Kolesnikova L, Sauerhering L, Erbar S, Weingartl H, Maisner A.** 2013.  
384 Nipah virus entry and egress from polarized epithelial cells. *J Virol* **87:3143-3154.**

- 385 15. **Bauer A, Neumann S, Karger A, Henning AK, Maisner A, Lamp B, Dietzel E, Kwasnitschka L,**  
386 **Balkema-Buschmann A, Keil GM, Finke S.** 2014. ANP32B is a nuclear target of henipavirus M  
387 proteins. *PLoS One* **9**:e97233.
- 388 16. **Pentecost M, Vashisht AA, Lester T, Voros T, Beaty SM, Park A, Wang YE, Yun TE, Freiberg**  
389 **AN, Wohlschlegel JA, Lee B.** 2015. Evidence for ubiquitin-regulated nuclear and subnuclear  
390 trafficking among Paramyxovirinae matrix proteins. *PLoS Pathog* **11**:e1004739.
- 391 17. **Wang YE, Park A, Lake M, Pentecost M, Torres B, Yun TE, Wolf MC, Holbrook MR, Freiberg**  
392 **AN, Lee B.** 2010. Ubiquitin-regulated nuclear-cytoplasmic trafficking of the Nipah virus matrix  
393 protein is important for viral budding. *PLoS Pathog* **6**:e1001186.
- 394 18. **Sun W, McCrory TS, Khaw WY, Petzing S, Myers T, Schmitt AP.** 2014. Matrix proteins of  
395 Nipah and Hendra viruses interact with beta subunits of AP-3 complexes. *J Virol* **88**:13099-  
396 13110.
- 397 19. **Patch JR, Han Z, McCarthy SE, Yan L, Wang LF, Harty RN, Broder CC.** 2008. The YPLGVG  
398 sequence of the Nipah virus matrix protein is required for budding. *Virol J* **5**:137.
- 399 20. **Cathomen T, Mrkic B, Spehner D, Drillien R, Naef R, Pavlovic J, Aguzzi A, Billeter MA,**  
400 **Cattaneo R.** 1998. A matrix-less measles virus is infectious and elicits extensive cell fusion:  
401 consequences for propagation in the brain. *Embo J* **17**:3899-3908.
- 402 21. **Mitra R, Baviskar P, Duncan-Decocq RR, Patel D, Oomens AG.** 2012. The human respiratory  
403 syncytial virus matrix protein is required for maturation of viral filaments. *J Virol* **86**:4432-  
404 4443.
- 405 22. **Thiel L, Diederich S, Erbar S, Pfaff D, Augustin HG, Maisner A.** 2008. Ephrin-B2 expression  
406 critically influences Nipah virus infection independent of its cytoplasmic tail. *Virol J* **5**:163.
- 407 23. **Yoneda M, Guillaume V, Sato H, Fujita K, Georges-Courbot MC, Ikeda F, Omi M, Muto-**  
408 **Terao Y, Wild TF, Kai C.** 2010. The nonstructural proteins of Nipah virus play a key role in  
409 pathogenicity in experimentally infected animals. *PLoS One* **5**:e12709.
- 410 24. **Mathieu C, Guillaume V, Volchkova VA, Pohl C, Jacquot F, Looi RY, Wong KT, Legras-**  
411 **Lachuer C, Volchkov VE, Lachuer J, Horvat B.** 2012. Nonstructural Nipah virus C protein  
412 regulates both the early host proinflammatory response and viral virulence. *J Virol* **86**:10766-  
413 10775.
- 414 25. **Ciancanelli MJ, Volchkova VA, Shaw ML, Volchkov VE, Basler CF.** 2009. Nipah virus  
415 sequesters inactive STAT1 in the nucleus via a P gene-encoded mechanism. *J Virol* **83**:7828-  
416 7841.
- 417 26. **Yun T, Park A, Hill TE, Pernet O, Beaty SM, Juelich TL, Smith JK, Zhang L, Wang YE, Vigant F,**  
418 **Gao J, Wu P, Lee B, Freiberg AN.** 2015. Efficient Reverse Genetics Reveals Genetic  
419 Determinants of Budding and Fusogenic Differences between Nipah and Hendra Viruses and  
420 Enables Real-Time Monitoring of Viral Spread in Small Animal Models of Henipavirus  
421 Infection. *J Virol* **89**:1242-1253.
- 422 27. **Radecke F, Spielhofer P, Schneider H, Kaelin K, Huber M, Dotsch C, Christiansen G, Billeter**  
423 **MA.** 1995. Rescue of measles viruses from cloned DNA. *Embo J* **14**:5773-5784.
- 424 28. **von Messling V, Zimmer G, Herrler G, Haas L, Cattaneo R.** 2001. The hemagglutinin of canine  
425 distemper virus determines tropism and cytopathogenicity. *J Virol* **75**:6418-6427.

- 426 29. **Inoue M, Tokusumi Y, Ban H, Kanaya T, Shirakura M, Tokusumi T, Hirata T, Nagai Y, Iida A, Hasegawa M.** 2003. A new Sendai virus vector deficient in the matrix gene does not form virus particles and shows extensive cell-to-cell spreading. *J Virol* **77**:6419-6429.
- 427
- 428
- 429 30. **Hyatt AD, Zaki SR, Goldsmith CS, Wise TG, Hengstberger SG.** 2001. Ultrastructure of Hendra virus and Nipah virus within cultured cells and host animals. *Microbes Infect* **3**:297-306.
- 430
- 431 31. **Mottet G, Mühlemann A, Tapparel C, Hoffmann F, Roux L.** 1996. A Sendai virus vector leading to the efficient expression of mutant M proteins interfering with virus particle budding. *Virology* **221**:159-171.
- 432
- 433
- 434 32. **Mottet-Osman G, Iseni F, Pelet T, Wiznerowicz M, Garcin D, Roux L.** 2007. Suppression of the Sendai virus M protein through a novel short interfering RNA approach inhibits viral particle production but does not affect viral RNA synthesis. *J Virol* **81**:2861-2868.
- 435
- 436
- 437 33. **Zhang G, Zhang S, Ding B, Yang X, Chen L, Yan Q, Jiang Y, Zhong Y, Chen M.** 2014. A leucine residue in the C terminus of human parainfluenza virus type 3 matrix protein is essential for efficient virus-like particle and virion release. *J Virol* **88**:13173-13188.
- 438
- 439
- 440 34. **Harrison MS, Sakaguchi T, Schmitt AP.** 2010. Paramyxovirus assembly and budding: building particles that transmit infections. *Int J Biochem Cell Biol* **42**:1416-1429.
- 441
- 442 35. **Landowski M, Dabundo J, Liu Q, Nicola AV, Aguilar HC.** 2014. Nipah virion entry kinetics, composition, and conformational changes determined by enzymatic virus-like particles and new flow virometry tools. *J Virol* **88**:14197-14206.
- 443
- 444
- 445 36. **Dietzel E, Anderson DE, Castan A, von Messling V, Maisner A.** 2011. Canine distemper virus matrix protein influences particle infectivity, particle composition, and envelope distribution in polarized epithelial cells and modulates virulence. *J Virol* **85**:7162-7168.
- 446
- 447
- 448 37. **Mahapatra M, Parida S, Baron MD, Barrett T.** 2006. Matrix protein and glycoproteins F and H of Peste-des-petits-ruminants virus function better as a homologous complex. *J Gen Virol* **87**:2021-2029.
- 449
- 450
- 451 38. **Sharma LB, Ohgimoto S, Kato S, Kurazono S, Ayata M, Takeuchi K, Ihara T, Ogura H.** 2009. Contribution of matrix, fusion, hemagglutinin, and large protein genes of the CAM-70 measles virus vaccine strain to efficient growth in chicken embryonic fibroblasts. *J Virol* **83**:11645-11654.
- 452
- 453
- 454
- 455 39. **Cathomen T, Naim HY, Cattaneo R.** 1998. Measles viruses with altered envelope protein cytoplasmic tails gain cell fusion competence. *J Virol* **72**:1224-1234.
- 456
- 457 40. **Moll M, Klenk HD, Maisner A.** 2002. Importance of the cytoplasmic tails of the measles virus glycoproteins for fusogenic activity and the generation of recombinant measles viruses. *J Virol* **76**:7174-7186.
- 458
- 459
- 460 41. **Erbar S, Maisner A.** 2010. Nipah virus infection and glycoprotein targeting in endothelial cells. *Virol J* **7**:305.
- 461
- 462 42. **Weise C, Erbar S, Lamp B, Vogt C, Diederich S, Maisner A.** 2010. Tyrosine residues in the cytoplasmic domains affect sorting and fusion activity of the Nipah virus glycoproteins in polarized epithelial cells. *J Virol*.
- 463
- 464
- 465

466 **FIGURE LEGENDS**467 **Fig. 1. Characterization of recombinant eGFP-expressing wildtype and M protein-deleted**

468 **NiV. (A)** Schematic drawings of NiV, NiVeG, NiVeGΔM full-length genomes in the cDNA  
469 plasmids. For all plasmids, the T7 RNA polymerase promoter is located immediately  
470 upstream of the genome, while the hepatitis δ ribozyme and T7 terminator are located  
471 immediately downstream of the genome to ensure correct genomic ends.

472 **(B)** Comparison of wildtype NiV and NiVeG titers. Vero cells were infected with recombinant  
473 wildtype NiV and NiVeG at a multiplicity of infection (MOI) of 0.001. Cell-free virus was  
474 quantified by the limited dilution method at 24 and 48 h p.i., and titers are expressed as 50%  
475 tissue culture infectious doses (TCID<sub>50</sub>/ml) (n = 4). Error bars indicate the standard deviation.

476 **(C)** Comparative growth kinetics of NiVeG and NiVeGΔM. Vero cells were infected at a MOI  
477 of 0.001. Cell-free virus titers were determined at 0, 24, 48 and 72 h (n = 3). Dotted line  
478 indicates the detection limit (50 TCID<sub>50</sub>/ml). An unpaired t-test was used to examine the  
479 significance of differences from NiVeG, (\*\*). p < 0.01.

480 **(D)** Comparison of cell-free and cell-associated virus titers. Vero cells were infected with  
481 wildtype (wt) and M-deleted NiV (ΔM) at a MOI of 0.001. At 48 h p.i., cell supernatants were  
482 harvested, cleared and titrated (cell-free). Cells were scraped into OptiMEM, subjected to  
483 one freeze-thaw cycle, and virus titers were quantified (cell-associated).

484

485 **Fig. 2. Live-cell microscopy to monitor NiVeG and NiVeGΔM cell-to-cell fusion kinetics.**

486 Vero cells were infected with NiVeG and NiVeGΔM at a MOI of 0.005. Time-lapse microscopy  
487 was started 16 h later, and GFP fluorescence signals were recorded every 30 min with a Leica  
488 DMI6000B microscope. **(A)** Selected images of the same microscopic field are shown for the  
489 indicated time points. Magnification 200x. Bar, 100 μm. **(B)** Quantitative fusion kinetics.

490 Areas of single syncytia were measured at different time points after infection (n=12). To  
491 calculate the relative increase in size, the area of the syncytium after 17 h was set to 1.  
492 Significance of difference between NiVeG and NiVeGΔM,  $p < 0.1$ .

493 **(C)** Effect of NiVeG and NiVeGΔM infection on cell viability. MTT assays were performed with  
494 Vero cells infected at a MOI of 0.001 or 0.01 at 24 h and 48 h after infection. Data were  
495 normalized to uninfected cells. Mean and SD are shown. Student's t-test analysis did not  
496 reveal any statistically significant differences.

497

498 **Fig. 3. Comparison of particle infectivity, protein composition, protease resistance, and**  
499 **thermostability. (A)** Relative particle numbers and infectivity-to-particle ratios of NiVeG and  
500 NiVeGΔM. Cell-free virus titers were quantified, and RNA was isolated from 100  $\mu$ l  
501 supernatant of infected cells after 48 h. Genomic RNA was quantified by qRT-PCR using NiV-  
502 N specific primers. The relative particle/genome numbers ( $2^{-Ct}$ ) normalized to NiVeG (set as  
503 1) are shown in the left panel. The infectivity-to-particle ratio was calculated by dividing the  
504 titer (TCID<sub>50</sub>/ml) by genome numbers ( $2^{-Ct}$ ) and was normalized to the values obtained for  
505 NiVeG (set as 1) to get the relative particle infectivity (right panel). Error bars indicate the  
506 standard deviation (n = 3). Statistical significance; (\*\*\*)  $p < 0,001$ .

507 **(B, C)** Viral protein content in infected cells and purified particles. Infected Vero cells were  
508 lysed at 48 h after infection, and cell-free virus was purified from cell supernatants. For each  
509 virus, 2 % of the total cell lysates and 33 % of the purified particles were separated on 10%  
510 SDS-PAGE gels. **(B)** To specifically detect viral proteins, one gel was blotted to nitrocellulose.  
511 Viral proteins were detected by Western blot analysis using NiV-M, -F, and -G-specific  
512 antisera and HRP-conjugated secondary antibodies. Chemiluminescent signals were  
513 recorded with a Chemidoc system (upper panel). NiV-N protein was visualized with a

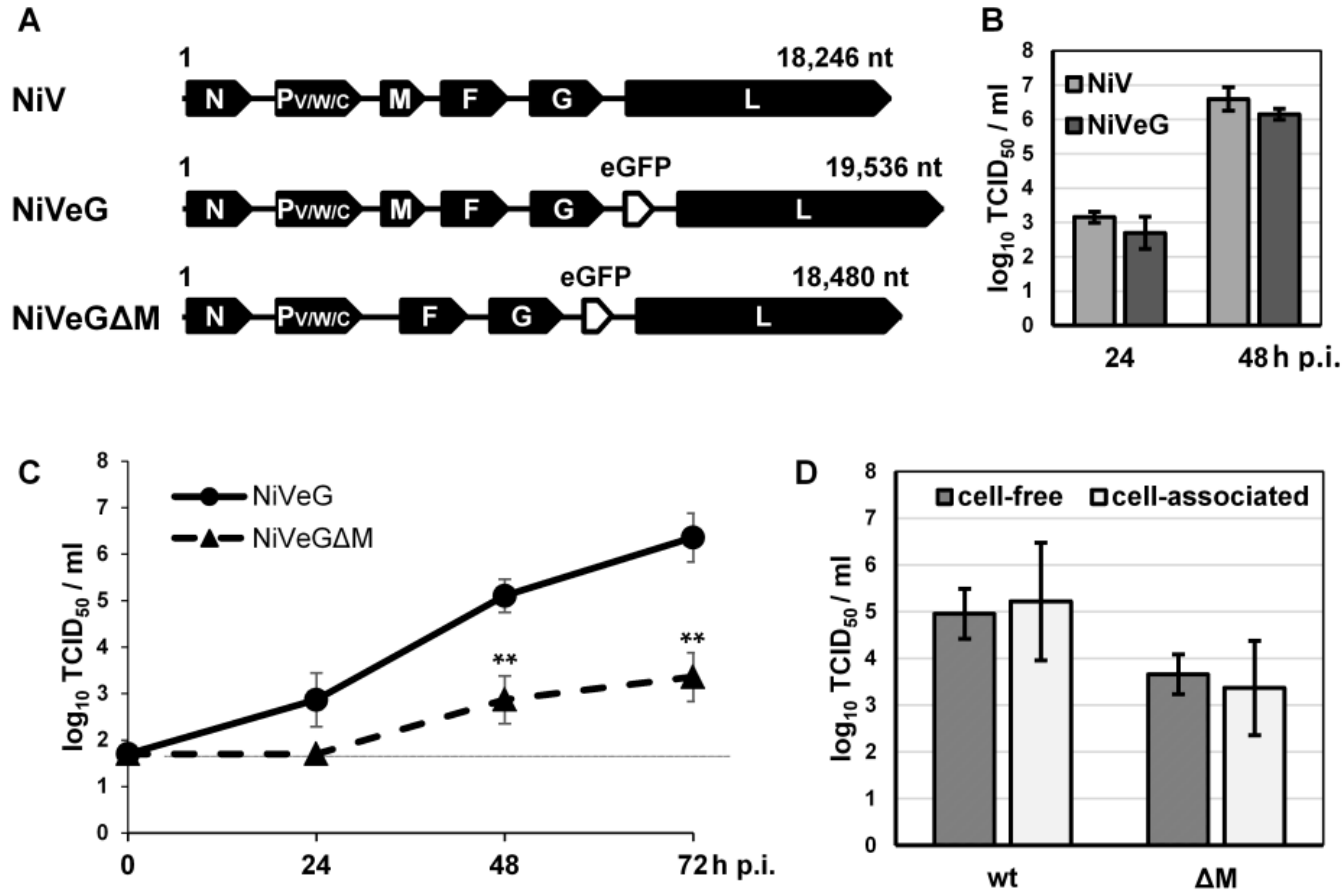
514 polyclonal NiV-specific guinea pig serum and IRDye700-labelled secondary antibodies.  
515 Signals were recorded with an Odyssey Imaging system (bottom panel). **(C)** To visualize all  
516 proteins in cell lysates and virus pellets, one gel was stained with Coomassie blue.

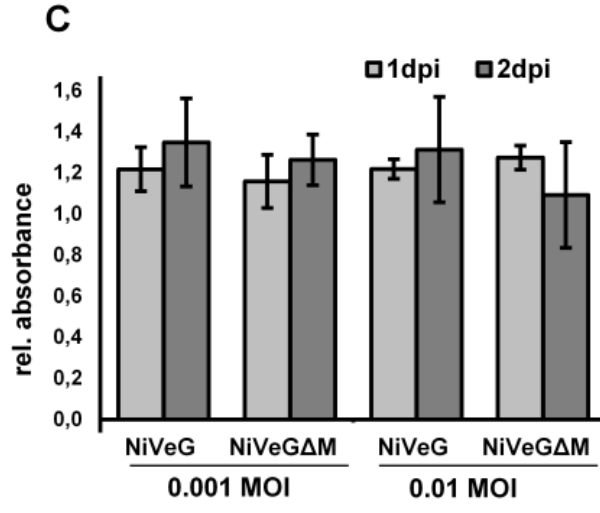
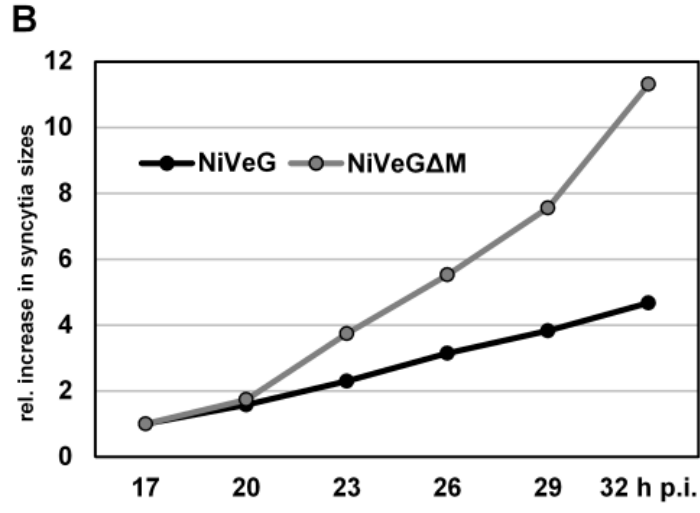
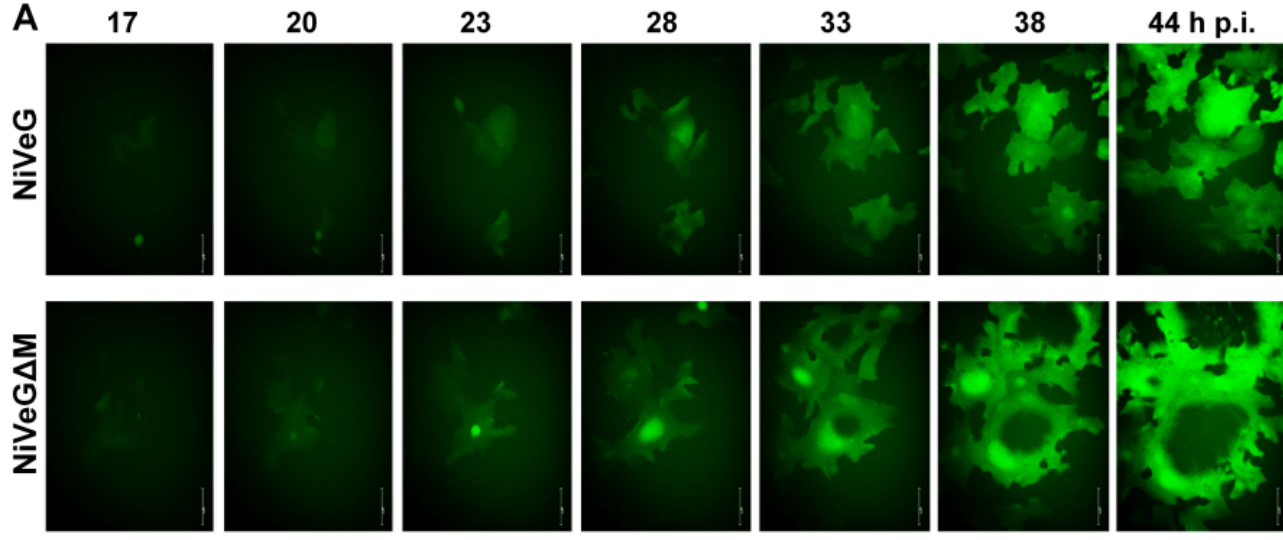
517 **(D)** Proteinase K protection assay. At 48 h after infection, virus particles were pelleted from  
518 clarified cell supernatants, suspended in PBS and either left untreated (w/o PK), or were  
519 treated with proteinase K in the absence (+PK) or presence of Triton X-100 (+PK/TX100). The  
520 samples were then analyzed by Western blot using polyclonal NiV-specific antibodies as  
521 described above.

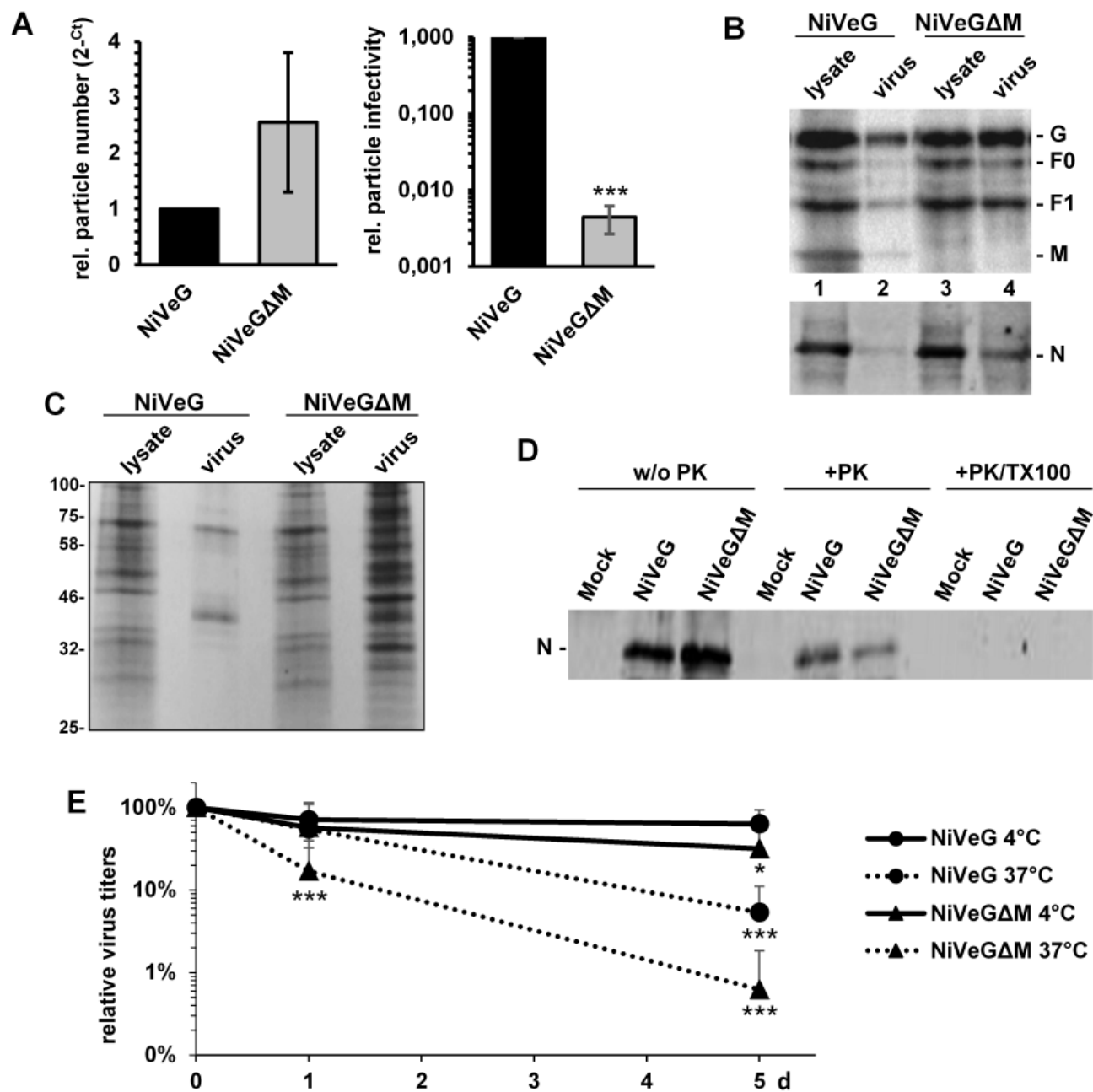
522 **(E)** Stability of NiVeG and NiVeGΔM infectivity at different temperatures. Cell-free virus was  
523 incubated for the indicated times at 4°C or 37°C, respectively. Titers at day 0 were set as  
524 100%, and used for the calculation of the relative loss in virus titers. Error bars indicate the  
525 standard deviation (n = 3). Statistical significance; (\*) p < 0.05, (\*\*\*) p < 0.001.

526

527 **Fig. 4. Ultrastructural analysis of viruses from cell supernatants.** Vero cells were infected  
528 with NiVeG and NiVeGΔM at a MOI of 0.005 for 48 h. Virus particles were purified from the  
529 supernatant by centrifugation over a 20% sucrose cushion, fixed and inactivated for 48 h in  
530 4% paraformaldehyde. **(A, B)** Samples were subjected to negative staining with 2%  
531 phosphotungstic acid. Bars, 1 μm. **(C-H)** Virus preparations were analyzed by  
532 immunoelectron microscopy using a NiV-specific polyclonal guinea pig antiserum and  
533 secondary antibodies coupled with 12 nm colloidal gold beads, followed by negative  
534 staining. **(C, D)** Spherical viral particles. Dashed lines indicate the positions of the measured  
535 diameters. **(E, F)** Filamentous viral particles. Arrows show defects in the integrity of virus  
536 envelope. **(G, H)** Pleomorphic particles. Arrowhead indicate membrane blebs. Bars, 200 nm.







NiVeG

NiVeGΔM

